Effective mass in bilayer graphene at low carrier densities: The role of potential disorder and electron-electron interaction

J. Li, L. Z. Tan, K. Zou, A. A. Stabile, D. J. Seiwell, K. Watanabe, T. Taniguchi, Steven G. Louie, and J. Zhu

Phys. Rev. B **94**, 161406 — Published 25 October 2016

DOI: 10.1103/PhysRevB.94.161406

Effective Mass in Bilayer Graphene at Low Carrier Densities: the Role of Potential Disorder and Electron-Electron Interaction

J. Li[1], L. Z. Tan[2,3†*], K. Zou[1‡], A. A. Stabile[1], D. J. Seiwell[1], K. Watanabe[4], T. Taniguchi[4], Steven G. Louie[2,3*], J. Zhu[1,5*]

[1]*Department of Physics, The Pennsylvania State University, University Park, Pennsylvania 16802, USA*

[2]*Department of Physics, University of California at Berkeley, Berkeley, California 94720, USA*

[3]*Materials Sciences Division, Lawrence Berkeley National Laboratory, Berkeley, California 94720, USA*

[4]*National Institute for Material Science, 1-1 Namiki, Tsukuba 305-0044, Japan*

[5]*Center for 2-Dimensional and Layered Materials, The Pennsylvania State University, University Park, Pennsylvania 16802, USA*

[†]Current address: *The Makineni Theoretical Laboratories, Department of Chemistry, University of Pennsylvania, Philadelphia, Pennsylvania 19104-6323, USA*

[‡]Current address: *Department of Applied Physics and Center for Research on Interface Structures and Phenomena (CRISP), Yale University, New Haven, Connecticut 06520, USA*

*Corresponding to: jzhu@phys.psu.edu (J. Zhu), sglouie@berkeley.edu (S. G. Louie), and liangtan@sas.upenn.edu (L. Z. Tan)

Abstract

In a two-dimensional electron gas, the electron-electron interaction generally becomes stronger at lower carrier densities and renormalizes the Fermi liquid parameters such as the effective mass of carriers. We combine experiment and theory to study the effective masses of electrons and holes m^*_e and m^*_h in bilayer graphene in the low carrier density regime of order 1×10^{11} cm^{-2}. Measurements use temperature-dependent low-field Shubnikov-de Haas (SdH) oscillations are made on high-mobility hexagonal boron nitride (h-BN) supported samples. We find that while m^*_e follows a tight-binding description in the whole density range, m^*_h starts to drop rapidly below the tight-binding description at carrier density $n = 6 \times 10^{11}$ cm^{-2} and exhibits a strong suppression of 30% when n reaches 2×10^{11} cm^{-2}. Contributions from electron-electron interaction alone, evaluated using several different approximations, cannot explain the experimental trend. Instead, the effect of potential fluctuation and the resulting electron-hole puddles play a crucial role. Calculations including both electron-electron interaction and disorder effects explain the experimental data qualitatively and quantitatively. This study reveals an unusual disorder effect unique to two-dimensional semi-metallic systems.

Bilayer graphene is a unique two-dimensional electron gas (2DEG) system with unusual electronic properties [1]. At high carrier densities, its hyperbolic bands are well described by a four-band Hamiltonian [2, 3] given by the tight-binding (TB) description [4], where the hopping parameters are determined by experiments or first-principles calculations [5-10]. Close to the charge neutrality point (CNP), bilayer graphene exhibits fascinating electron-electron (e-e) interaction driven ground states [11-15]. A natural question arises: How does the density of states of bilayer graphene near the Fermi energy evolve as carrier density n decreases continuously? The study of the effective carrier mass m^* is a powerful tool to probe this evolution. Indeed, in conventional 2DEGs, increasing e-e interaction leads to substantial increase of m^* at low carrier densities, long before predicated many-body instabilities [16-21]. Such studies provide valuable inputs to advance many-body calculations [22]. In monolayer and bilayer graphene, the proximity of the conduction and valence bands and their pseudospin characters, play a significant role in the screening of the Coulomb interaction. This has consequences for the dispersions of the elementary excitations and the transport properties of these systems [23-26]. In monolayer graphene, both calculations[27], and measurements of m^* [28] [29] report strong enhancement of the Fermi velocity v_F at low carrier densities. In comparison, the situation in bilayer graphene is much less clear. Existing theoretical predictions vary greatly on the sign and magnitude of the interaction correction to m^* [30-35] while measurements have been lacking.

In our earlier work [10], we reported on the measurements of m^* of bilayer graphene in the density regime of order 1×10^{12} cm^{-2}. A TB description was found to work well, the hopping parameters of which were accurately extracted from data. As the previous samples rested on oxides, disorder (field effect mobility μ_{FE} ~ a few thousand cm^{2}V^{-1}s^{-1} and disorder energy δE of a few tens of meV [36, 37]) prevented measurements at lower densities. In our current h-BN supported samples, μ_{FE} reaches 30,000 cm^{2}V^{-1}s^{-1}, which allows for precise determination of m^* down to $n = 2 \times 10^{11}$ cm^{-2} for both electrons and holes. Following the conventional definition of the interaction parameter $r_s = U/E_F$, where U is the Coulomb interaction energy $e^2\sqrt{n\pi}/(4\pi\varepsilon_0\varepsilon)$ and E_F is the Fermi energy, we estimate r_s to be $7.5/\sqrt{n(\text{in unit of } 10^{11}\text{cm}^{-2})}$ using $m^* = 0.033$ m$_e$, which is the average value of the measured electron and hole masses near 1×10^{12} cm^{-2} in Ref. [10]. In our present studied carrier density regime ($2 - 12 \times 10^{11}$ cm^{-2}), r_s ranges from 2.2 to 5.3, which is quite large compared to GaAs 2DEG, where the renormalized m^* exceeds the band mass by 40% at $r_s \sim 5$ due to e-e interaction [18]. Here, we find that m^*_e and m^*_h behave very differently as n decreases. While m^*_e continues to follow the high-density TB extrapolation, m^*_h sharply dives in value below $n = 6 \times 10^{11}$ cm^{-2}, reaching about 70% of the TB band mass at $n = 2 \times 10^{11}$ cm^{-2}. A thorough theoretical investigation evaluating the effect of e-e interaction in different approximations, together with the effect of Coulomb potential disorder, identifies density inhomogeneity to be a key factor in explaining the experimental observations. This unusual effect of disorder is unique to 2D semi-metallic systems.

Bilayer Hall bar-like devices are made by exfoliating, transferring, stacking and patterning of multi-layer-graphene bottom gate electrode, 15 – 30nm thick h-BN gate dielectric (Momentive, Polartherm grade PT110 and NIMS) and bilayer graphene sheet (Kish Graphite) using a PMMA/PVA based transfer method [38] and standard e-beam lithography. Transport experiments are carried out in a variable-temperature, pumped He^4 cryostat with a 9 T magnet using standard low-frequency lock-in technique (47 Hz) with current excitation 50 nA. Figure 1 plots the sheet resistance vs carrier density $R_{\text{sheet}}(n)$ of samples A and B, together with sample C reported in Zou et al [10] for comparison. The field effect mobility μ_{FE} is 30,000 $\text{cm}^2\text{V}^{-1}\text{s}^{-1}$ and 22,000 $\text{cm}^2\text{V}^{-1}\text{s}^{-1}$ respectively in samples A and B, in comparison to μ_{FE} = 4,000 $\text{cm}^2\text{V}^{-1}\text{s}^{-1}$ in sample C, which is supported on SiO_2 substrate. The unintentional doping for both devices are moderate, and the effect of the displacement (D) field on the bare band mass is modeled in S4 of the supplementary material for both devices [39]. We find that the presence of a small D-field does not change the conclusions of the paper.

The effective mass m^* as measured in quantum oscillations is given by

$$m^* = \frac{\hbar^2}{2\pi}\frac{dA(E)}{dE}\Big|_{E=E_F} \qquad (1)$$

where $A(E)$ is the k-space area enclosed by the contour of constant energy E in the quasi-particle band structure. To accurately determine m^*, we measure the temperature-dependent magneto-resistance $R_{xx}(B)$ at a fixed carrier density (Fig. 2(a)), extract the low-field Shubnikov de Haas (SdH) oscillation amplitude $\delta R_{xx}(T, B)$ and perform simultaneous fitting of the temperature and magnetic field dependence to the Lifshitz-Kosevich formula[40],

$$\frac{\delta R_{xx}}{R_0} = 4\gamma_{th}\exp\left(\frac{-\pi}{\omega_c\tau_q}\right), \gamma_{th} = \frac{2\pi^2 k_B T/\hbar\omega_c}{sinh(2\pi^2 k_B T/\hbar\omega_c)} \qquad (2)$$

where $\omega_c = \frac{eB}{m^*}$ is the cyclotron frequency. The effective mass m^* and the quantum scattering time τ_q are the two fitting parameters.

This global fitting procedure is illustrated in Figs. 2(b) and (c) for two carrier densities n_h = 4.7 and 3.0 × 10^{11} cm^{-2} as examples (see S1 and S2 of the supplementary material [39]). Compared to common practice of approximating δR_{xx} at a fixed B-field by linearly interpolating adjacent peak heights and analyze its T-dependence to obtain m^*, fits to Eq. (2) better represent the oscillation amplitude δR_{xx}, especially at low carrier densities when only a few oscillations are available (See Fig. 2(c) for example). It also enables us to discern and avoid using the T-dependent oscillations of nascent quantum Hall states, the analysis of which can lead to error in m^* (see caption in Fig. 2(b)). The effective mass m^* obtained using the global fitting procedure is B-independent and best extrapolates to the density-of-states mass of the bilayer graphene at B = 0, which is expected to be modified by e-e interactions [30-35].

The above analysis enables us to accurately determine both the electron and hole effective mass m^*_h and m^*_e for the approximate carrier density range of 1 - 10 × 10^{11}cm^{-2}. The uncertainty of m^* varies from ± 0.0002 m_e to ± 0.004 m_e from high to low densities. The high accuracy of the measurements facilitates comparison to theory as interaction corrections to m^* are expected to be typically in the few to tens of percent range [16, 18]. Also plotted in Fig. 2(d) is the quantum scattering time τ_q in both samples. τ_q is between 100 and 140 fs for both electrons and holes. Compared to ~ 40 fs in sample C [10], the high τ_q values of samples A and B attest to the improvement of sample quality. Below n =1 × 10^{11} cm^{-2}, the SdH oscillations become increasingly more non-sinusoidal due to density inhomogeneity and global fits cannot be obtained reliably.

Figure 3 plots m^*_h and m^*_e obtained in samples A and B, together with data from sample C in Ref. [10]. In the overlapping density regime, current and previous results agree very well and are well described by the TB model with hopping parameters γ_0 = 3.43 eV, γ_1 = 0.40 eV γ_3 = 0 and v_4 = γ_4/γ_0 = 0.063, Δ = 0.018 eV, which are determined in Ref. [10]. The calculated m^* are plotted as dashed lines in Fig. 3. The electron and hole branches use the same set of parameters, with their mass differences captured by v_4. On the electron side, the TB parameters continue to describe all the m^*_e data very well down to the lowest density measured. On the hole side, however, m^*_h exhibits a sharp drop from the TB model as n_h is decreased to less than 5 × 10^{11} cm^{-2}, reaching a large suppression of 30% at n_h = 2 × 10^{11} cm^{-2}. These densities are still sufficiently high that the effect of trigonal warping [1] can be safely neglected. (Fig. S6 of the supplementary material [39])

In existing theoretical studies of bilayer electronic dispersions, the effect of e-e interaction manifests in two ways, *i. e.* by renormalizing the hopping parameters within the TB model at high carrier densities [33] and by causing deviations of m^* from the TB description at low carrier densities, with different trends of m^* predicted [30-32, 34, 35]. We begin our calculations with a four-band TB Hamiltonian with non-interacting hopping parameters and explicitly include e-e interaction with the random phase approximation (RPA) of the screened exchange self-energy

$$\Sigma(k) = -\sum_q \frac{V^{2D}(q)}{\varepsilon(q)} F^{ss'}(k, k+q) \qquad (3)$$

using a dielectric function $\varepsilon(q) = \varepsilon_{BN} - V^{2D}(q)\chi(q)$, that includes contributions from both the bilayer graphene and the h-BN substrate and overlayer. Here $\varepsilon_{BN} = 3.0$ is determined from the gating efficiency of the backgate, and $F^{ss'}$ is the pseudospin overlap factor [30, 31]. Eq. (3) provides the RPA correction to the bare energy bands $E_0(k)$ obtained from TB calculation to yield the quasiparticle band structure $E(k) = E_0(k) + \Sigma(k)$. The effective mass is then computed using Eq. (1).

The calculated m^*_e and m^*_h are plotted in Fig. 4 in olive dotted lines. Interaction leads to a slightly faster decrease of m^*_e and m^*_h at low carrier densities, in contrast to the sudden drop

observed in the measured m^*_h for $n_h < 5 \times 10^{11}$ cm^{-2}. Examining the problem from a different angle, we note that in the RPA model, the dielectric function is well described by the Thomas-Fermi (TF) screening $\varepsilon(q) = \varepsilon_{BN} + \frac{q_{TF}}{q}$ in the small q limit [34]. Fitting the TF description to our data yields a ten-fold reduction of the TF screening wavevector q_{TF} from its expected value of $q_{TF} = m^* e^2/\hbar^2$. This would imply extremely weak screening of the e-e interaction in our devices, which cannot be justified. (see Fig. S7 of the supplementary material [39]). Thus, e-e interaction effect, at least at the RPA level, appears to be too weak to account for the experimental observations. In comparison, in monolayer graphene, a large suppression of m^* is also observed at low carrier densities and well described by RPA calculations [28].

Can Coulomb potential fluctuation and the resulting density inhomogeneity[36, 37, 41] play a role? The answer is not so intuitive at the first glance. In a conventional semiconducting 2DEG, density inhomogeneity results in the smearing of $m^*(n)$. This effect does not alter the trend of $m^*(n)$ and is typically non-consequential in the carrier density regime where the SdH oscillations are well-behaved. In Fig. 2(c)), the SdH oscillations at $n_h = 3 \times 10^{11}$ cm^{-2} appear to be well-behaved, yet the measured m^*_h is already 14% below the TB band mass. Here, the *gapless* nature of the bilayer bands makes a crucial difference between bilayer graphene and a conventional 2DEG. As the inset of Fig. 4 illustrates, as the Fermi energy E_F approaches the disorder energy scale δE, instead of depletion, carriers of the opposite sign start to appear in parts of the sample. The SdH oscillations of a minority carrier type have the opposite sign in dA/dE; their presence in some regions of the sample therefore contributing negatively to the average of m^*, resulting in a decrease in its value. Such cancellation effect does not occur in a conventional semiconductor 2DEG.

This situation can be modeling by defining the overall carrier density and effective mass as ensemble averages of their local counterparts n_{loc} and m_{loc} respectively:

$$n(E) = \langle n_{loc} \rangle = \int d\mu \, f(\mu) \, n_{loc}(E + \mu) \qquad (4)$$

$$m(E) = \langle m_{loc} \rangle = \int d\mu \, f(\mu) \, m_{loc}(E + \mu) \qquad (5)$$

Here, the fluctuation of energy is assumed to have a Gaussian profile $f(\mu)$ with standard deviation δE.

Effective masses calculated using the RPA model and including disorder characterized by a broadening energy $\delta E = 5.4$ meV are plotted as solid lines in Fig. 4. Evidently, the combination of e-e interaction and Coulomb potential fluctuations can now quantitatively reproduce the observed behavior of m^*_e and m^*_h over the entire range of measurement and for both samples. Remarkably, the same value for δE simultaneously captures the sharp decrease of m^*_h at $n_h < 5 \times 10^{11}$ cm^{-2} and the absence of such decrease on the electron side. Our calculations predict that m^*_e should also substantially decrease from the TB values at yet lower carrier densities, just below the range probed in our measurements. The difference arises from a smaller electron density inhomogeneity due to a smaller m^*_e. The quantum scattering time $\tau_q \sim 120$ fs found in both

samples (Fig. 2(d)) yields $\delta E \sim \hbar/2\tau_q \sim 2.7$ meV, in good agreement with the theoretical fit. In addition, we can estimate the density fluctuation δn by locating the onset density n^* at which the conductance sharply increases with density [11-15]. n^* is approximately 2×10^{10} cm^{-2} in sample A and 4×10^{10} cm^{-2} in sample B (Fig. S4). These values are also consistent with estimates obtained by locating the crossover density $n(\mathrm{h/e})_c \sim 5 \times 10^{10}$ cm^{-2}, where the temperature dependence of $R(n)$ changes from that of a metal, *i. e*. $dR/dT > 0$ to that of an insulator, *i. e.* $dR/dT < 0$ [42] in a bilayer sample of similar quality. A δn of 5×10^{10} cm^{-2} corresponds to $\delta E = 2$ meV using $m^* = 0.03$ m$_e$. These consistent estimates of disorder energy scales support the fitting value of δE used for both samples. Furthermore, our calculations also show that interaction renormalizes the inter-band transition energy γ_1 from the "bare" value of 0.36 eV (Fig. 4) to 0.38 eV, in excellent agreement with infra-red absorption measurements [6, 7, 9].

In Ref. [10], we have shown that a set of renormalized TB hopping parameters can capture m^* in the high-density regime very well, without explicitly including e-e interactions (See dashed lines in Fig. 3). In Fig. S8 of the supplementary material [39], we show that adding disorder broadening δE to this set of parameters can also capture the main trend of data, with the diving of m^*_h at low densities slightly too abrupt compared to experiment.

The above studies highlight a few remarkable differences between bilayer graphene, a gapless Dirac Fermi liquid and conventional semiconductor 2DEGs. Firstly, both our calculations and measurements suggest that the effect of e-e interaction on m^* in bilayer graphene remains weak down to $n \sim 2 \times 10^{11}$ cm^{-2} ($r_s = 5.3$) while past studies on GaAs electrons showed an enhancement of more than 40% at this interaction parameter [18]. Secondly, the effect of disorder appears quite different in these two systems. In conventional semiconducting 2DEGs, disorder leads to localization and therefore the *increase*, rather than the decrease of m^* at low carrier densities [18]. Here in gapless bilayer graphene, disorder leads to coexisting electrons and holes and consequently a partial cancellation effect on m^*. In comparison to the well-recognized Klein tunneling effect in p-n junctions [43, 44], this study exposed a more elusive effect of electron-hole puddle. Studies of low-carrier-density regimes in Dirac materials thus require a great deal of caution. For now, samples of yet higher qualities are necessary to elucidate the intrinsic behavior of m^* near the charge neutral point of bilayer graphene.

In conclusion, we have performed careful measurements of the effective mass m^* in high-quality h-BN supported bilayer graphene samples down to the carrier density regime of 1×10^{11} cm^{-2} and observed sharp decrease of the hole mass at low carrier densities. Our calculations show that while the inclusion of electron-electron interaction is necessary to reach excellent quantitative agreement with data at all carrier densities, Coulomb potential fluctuations, which result in the co-existence of electron and hole regions and a partial cancellation of m^*, is chiefly responsible for the observed sharp drop in m^*_h at low densities. This mechanism, which is absent in finite-gap semiconductor two-dimensional systems, is another manifestation of the unusual consequences of gapless Dirac bands.

Acknowledgement

J. L., K. Z., A. A. S. D. J. S. and J. Z. are supported by NSF under Grants CAREER No. DMR-0748604 and No. DMR-1506212 and by ONR under Grant No. N00014-11-1-0730. L. Z. T. and S. G. L. are supported by the Theory Program at the Lawrence Berkeley National Lab through the Office of Basic Energy Sciences, U.S. Department of Energy under Contract No. DE-AC02-05CH11231 which provided theoretical analyses and simulations of disorder effects; and by the National Science Foundation under Grant No. DMR15-1508412 which provided for the calculation of electron-electron interaction effects. K. W. and T. T. are supported by the Elemental Strategy Initiative conducted by the MEXT, Japan. T. T. is also supported by a Grant-in-Aid for Scientific Research on Grant 262480621 and on Innovative Areas "Nano Informatics" (Grant No. 25106006) from JSPS. The authors acknowledge use of facilities at the PSU site of NSF NNIN. We are grateful for helpful discussions with X. Hong.

Reference

[1] M. Edward and K. Mikito, Rep. Prog. Phys. **76**, 056503 (2013).
[2] M. Mucha-Kruczynski, E. McCann, and V. I. Fal'ko, Semicond. Sci. Technol. **25**, 033001 (2010).
[3] J. Nilsson, A. H. Castro Neto, F. Guinea, and N. M. R. Peres, Physical Review B **78**, 045405 (2008).
[4] J. Jung and A. H. MacDonald, Physical Review B **89**, 035405 (2014).
[5] E. A. Henriksen and J. P. Eisenstein, Physical Review B **82**, 041412 (2010).
[6] A. B. Kuzmenko, I. Crassee, D. van der Marel, P. Blake, and K. S. Novoselov, Physical Review B **80**, 165406 (2009).
[7] Z. Q. Li, E. A. Henriksen, Z. Jiang, Z. Hao, M. C. Martin, P. Kim, H. L. Stormer, and D. N. Basov, Physical Review Letters **102**, 037403 (2009).
[8] L. M. Malard, J. Nilsson, D. C. Elias, J. C. Brant, F. Plentz, E. S. Alves, A. H. Castro Neto, and M. A. Pimenta, Physical Review B **76**, 201401 (2007).
[9] L. M. Zhang, Z. Q. Li, D. N. Basov, M. M. Fogler, Z. Hao, and M. C. Martin, Physical Review B **78**, 235408 (2008).
[10] K. Zou, X. Hong, and J. Zhu, Physical Review B **84**, 085408 (2011).
[11] P. Maher, C. R. Dean, A. F. Young, T. Taniguchi, K. Watanabe, K. L. Shepard, J. Hone, and P. Kim, Nature Physics **9**, 154 (2013).
[12] J. Velasco, Jr. *et al.*, Nature Nanotechnology **7**, 156 (2012).
[13] A. S. Mayorov *et al.*, Science **333**, 860 (2011).
[14] R. T. Weitz, M. T. Allen, B. E. Feldman, J. Martin, and A. Yacoby, Science **330**, 812 (2010).
[15] B. E. Feldman, J. Martin, and A. Yacoby, Nature Physics **5**, 889 (2009).
[16] Y. W. Tan, J. Zhu, H. L. Stormer, L. N. Pfeiffer, K. W. Baldwin, and K. W. West, Physica E **34**, 260 (2006).
[17] R. Asgari, B. Davoudi, M. Polini, G. F. Giuliani, M. P. Tosi, and G. Vignale, Physical Review B **71**, 045323 (2005).
[18] Y. W. Tan, J. Zhu, H. L. Stormer, L. N. Pfeiffer, K. W. Baldwin, and K. W. West, Physical Review Letters **94**, 016405 (2005).
[19] S. V. Kravchenko and M. P. Sarachik, Rep. Prog. Phys. **67**, 1 (2004).
[20] V. M. Pudalov, M. E. Gershenson, H. Kojima, N. Butch, E. M. Dizhur, G. Brunthaler, A. Prinz, and G. Bauer, Physical Review Letters **88**, 196404 (2002).

[21] Y. K. Kwon, D. M. Ceperley, and R. M. Martin, Physical Review B **50**, 1684 (1994).
[22] G. Giuliani and G. Vignale, *Quantum Theory of the Electron Liquid* (Cambridge University Press, 2005).
[23] E. H. Hwang and S. Das Sarma, Physical Review B **75**, 205418 (2007).
[24] M. Polini, R. Asgari, G. Borghi, Y. Barlas, T. Pereg-Barnea, and A. H. MacDonald, Physical Review B **77**, 081411 (2008).
[25] C.-H. Park, F. Giustino, C. D. Spataru, M. L. Cohen, and S. G. Louie, Nano Lett. **9**, 4234 (2009).
[26] S. Das Sarma, S. Adam, E. H. Hwang, and E. Rossi, Reviews of Modern Physics **83**, 407 (2011).
[27] V. N. Kotov, B. Uchoa, V. M. Pereira, F. Guinea, and A. H. Castro Neto, Reviews of Modern Physics **84**, 1067 (2012).
[28] D. C. Elias *et al.*, Nature Physics **7**, 701 (2011).
[29] D. A. Siegel, C.-H. Park, C. Hwang, J. Deslippe, A. V. Fedorov, S. G. Louie, and A. Lanzara, Proceedings of the National Academy of Sciences **108**, 11365 (2011).
[30] A. Sabashvili, S. Ostlund, and M. Granath, Physical Review B **88**, 085439 (2013).
[31] R. Sensarma, E. H. Hwang, and S. Das Sarma, Physical Review B **84**, 041408 (2011).
[32] Y. Lemonik, I. L. Aleiner, C. Toke, and V. I. Fal'ko, Physical Review B **82**, 201408 (2010).
[33] P. Gava, M. Lazzeri, A. M. Saitta, and F. Mauri, Physical Review B **79**, 165431 (2009).
[34] G. Borghi, M. Polini, R. Asgari, and A. H. MacDonald, Solid State Communications **149**, 1117 (2009).
[35] S. V. Kusminskiy, D. K. Campbell, and A. H. Castro Neto, Europhysics Letters **85**, 58005, 58005 (2009).
[36] K. Zou and J. Zhu, Physical Review B **82**, 081407 (2010).
[37] A. Deshpande, W. Bao, Z. Zhao, C. N. Lau, and B. J. LeRoy, Applied Physics Letters **95**, 243502 (2009).
[38] C. R. Dean *et al.*, Nature Nanotechnology **5**, 722 (2010).
[39] See Supplemental Material at [URL will be inserted by publisher] for more details about global fitting procedure, estimation of density fluctuation, effects of band gap and trigonal warping on m^* and more theoretical fits.
[40] D. Shoenberg, *Magnetic Oscillations in Metals* (Cambridge University Press, 1984).
[41] M. Yankowitz, J. Xue, and B. J. LeRoy, Journal of Physics-Condensed Matter **26**, 303201 (2014).
[42] C. Cobaleda, S. Pezzini, E. Diez, and V. Bellani, Physical Review B **89**, 121404 (2014).
[43] A. F. Young and P. Kim, Annual Review of Condensed Matter Physics **2**, 101 (2011).
[44] V. V. Cheianov and V. I. Fal'ko, Physical Review B **74**, 041403 (2006).

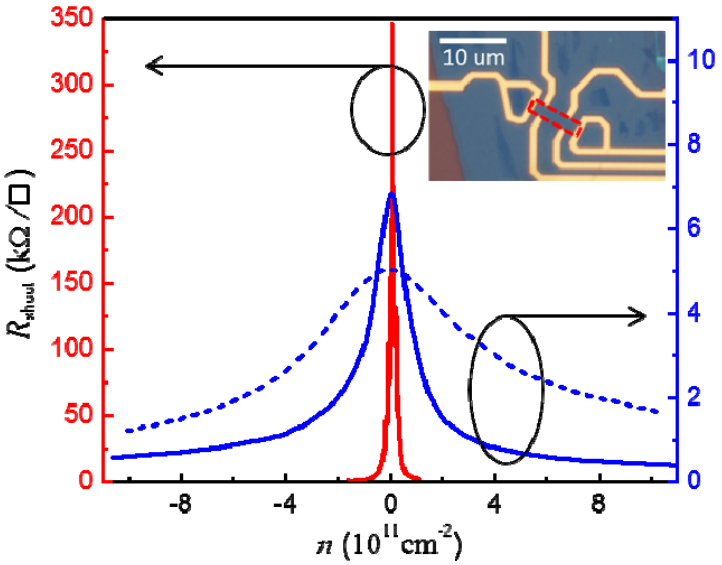

FIG. 1. Sheet resistance vs carrier density R_{sheet} (n) for samples A (solid red), B (solid blue) and C (dashed blue). Samples A and B are supported on h-BN, sample C on SiO_2. The field effect mobility μ_{FE} is 30,000 $cm^2V^{-1}s^{-1}$, 22,000 $cm^2V^{-1}s^{-1}$, and 4000 $cm^2V^{-1}s^{-1}$ respectively for samples A to C. T = 1.6 K. The large resistance sample A exhibits at the CNP results from a finite band gap caused by unintentional doping. We discuss the effect of a band gap on the band mass in S4 of the supplementary material [39]. Inset: An optical micrograph for sample A.

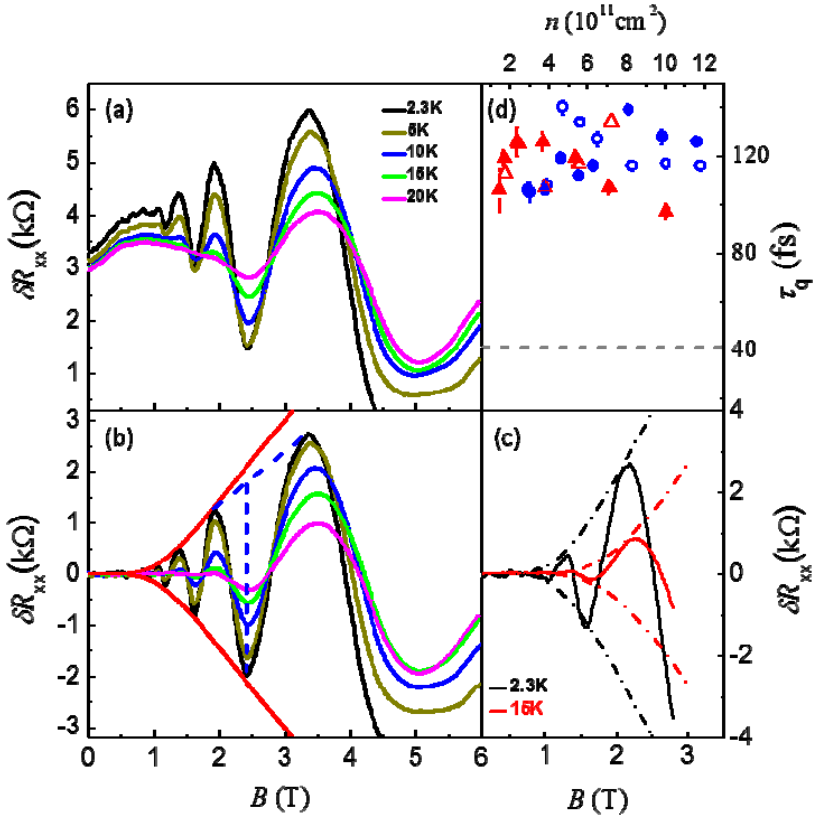

FIG. 2. (a) T-dependent magnetoresistance $R_{xx}(B)$ for $n_h = 4.7 \times 10^{11}$ cm^{-2} at selected temperatures as indicated in the plot. (b) Oscillation amplitude $\delta R_{xx}(B)$ of data in (a) after background subtraction. The solid red curve plots Eq.(1) with fitting parameters $m_h^* = 0.0347$ m_e and $\tau_q = 140$ fs. $T = 2.3$ K. $\delta R_{xx}(B)$ starts deviating from the fit above $B = 3$ T. Conventional method used to extract δR_{xx} is illustrated by the blue dashed lines and produces $m^* = 0.0311(2)$ m_e. This is 10% smaller than $m_h^* = 0.0347$ m_e obtained from the global fitting. (c) $\delta R_{xx}(B)$ for $n_h = 3.0 \times 10^{11}$ cm^{-2} at $T = 2.3$ K and $T = 15$ K. Dashed curves are fits to Eq.(2) with $m_h^* = 0.0285$ m_e and $\tau_q = 107$ fs. Data in (a)-(c) are from sample B. (d) The quantum scattering time τ_q as a function of carrier density in sample A (red symbols) and sample B (blue symbols). Electrons are shown in filled symbols and holes in open symbols. τ_q is about 40 fs (dashed grey line) in sample C (Ref. [10]).

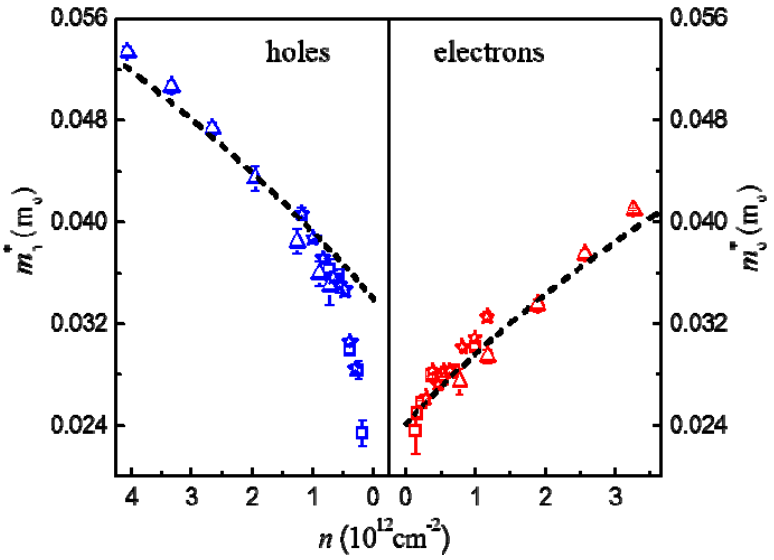

FIG. 3. The effective carrier mass m_h^* and m_e^* as a function of the carrier density (red for electrons, blue for holes) in samples A (squares), B (stars), and C (triangles). Data on C is from Ref. [10]. Together, the measurement covers the density range of approximately 1.4 - 41 × 10^{11} cm^{-2}. The dashed curves plot m^* calculated using a 4 × 4 tight-binding Hamiltonian with hopping parameters γ_0 = 3.43 eV, γ_1 = 0.40 eV, γ_3 = 0, and v_4 = 0.063. These values are obtained in Ref.[10] by fitting the data in sample C at high densities.

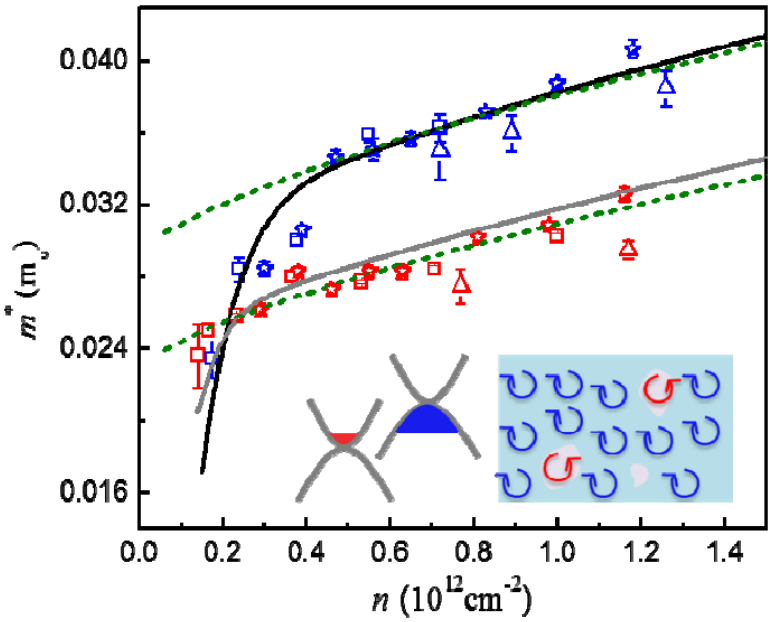

FIG. 4. Comparison of calculations and experiment at low carrier density ($0.2 - 1.3 \times 10^{12}$ cm^{-2}). Experimental data follow the symbols used in Fig. 3. The olive dashed lines plot the calculated m^* including e-e interaction in a random phase approximation. The black and gray lines are calculations that further include the effect of potential disorder using $\delta E = 5.4$ meV obtained from τ_q and the temperature dependence of the conductance. In both calculations, $\gamma_0 = 3.08$ eV and $\gamma_1 = 0.36$ eV are chosen to fit the experimental data in the high-density regime. Their values differ from those obtained in Ref. [10] since e-e interaction is explicitly calculated here whereas in Ref.[10] its effect is represented by renormalizing the hopping parameters. $\gamma_3 = 0$ and $\nu_4 = 0.063$ are taken from Ref. [10]. Inset: A schematic illustration of the electron-hole coexistence at low carrier densities due to disorder and its effect on the cyclotron motion.